

Spin Polarization of Fractional Quantum Hall States with $\nu < 2$

Shosuke Sasaki

Center for Advanced High Magnetic Field Science, Graduate School of Science, Osaka University, Osaka, Japan
Email: sasaki@mag.ahmf.sci.osaka-u.ac.jp, zazensou@gmail.com

Received 26 March 2015; accepted 22 May 2015; published 25 May 2015

Copyright © 2015 by author and Scientific Research Publishing Inc.
This work is licensed under the Creative Commons Attribution International License (CC BY).
<http://creativecommons.org/licenses/by/4.0/>



Open Access

Abstract

The spin polarization of a fractional quantum Hall state shows very interesting properties. The curve of polarization versus magnetic field has wide plateaus. The fractional quantum Hall effect is caused by the Coulomb interaction because the 2D electron system without the Coulomb interaction yields no energy gap at the fractional filling factor. Therefore, the wide plateau in the polarization curve is also caused by the Coulomb interaction. When the magnetic field is weak, some electrons have up-spins and the others down-spins. Therein the spin-exchange transition occurs between two electrons with up and down spins via the Coulomb interaction. Then the charge distribution before the transition is the same as one after the transition. So these two states have the same classical Coulomb energy. Accordingly, the partial Hamiltonian composed of the spin exchange interaction should be treated exactly. We have succeeded in diagonalizing the spin exchange interaction for the first and second nearest electron pairs. The theoretical results reproduce the wide plateaus very well. If the interval modulations between Landau orbitals are taken into the Hamiltonian, the total energy has the Peierls instability. We can diagonalize the Hamiltonian with the interval modulation. The results reproduce wide plateaus and small shoulders which are in good agreement with the experimental data.

Keywords

Spin Polarization, Fractional Quantum Hall Effect, 2D Electron System, Quantum Theory

1. Introduction

As well known, the integer and fractional quantum Hall effects (IQHE and FQHE) appear in a quasi-two dimensional electron system under a strong magnetic field perpendicular to the 2D electron channel the thickness of which is extremely thin [1]-[17]. Only the ground state along the z -direction of **Figure 1** is realized actually for a low temperature and so we can treat the system as a 2D electron system. The confinement of the Hall resistance

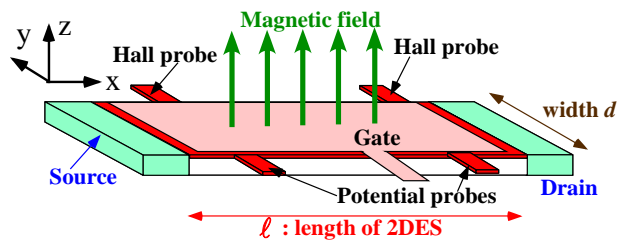


Figure 1. Quantum hall device.

at IQHE is extremely accurate and then the confined resistance is employed as the resistance standard [18]. The IQHE and FQHE are observed in various materials namely Si, GaAs, graphene and so on. The QHE appears independently of materials and is caused only by many electrons in a thin film. The Hall resistance is the ratio between Hall voltage and electric current. In the IQHE the Hall voltage is larger than about 10^{-4} Volts and the diagonal (potential) voltage is less than 10^{-11} Volt. Also in the FQHE the Hall voltage is extremely large compared with the potential voltage. Therefore this asymmetry of x and y directions in **Figure 1** should be taken into consideration in the investigations of QHE. Consequently the total Hamiltonian of many electrons should be composed of three kinds of interactions namely the strong magnetic field interaction, the Coulomb interactions between electrons, and the electric field produced by the Hall voltage. However, many theories ignore the electric field along the Hall voltage. We take account of the electric potential along the y -direction in **Figure 1**.

We have developed the theory of Tao and Thouless [19] [20] and have found out the most uniform configuration of electrons in the Landau orbitals which yields the minimum expectation value of the total Hamiltonian H_T [21]-[25]. Since the Coulomb interaction depends only upon the relative coordinate between two electrons, the x component of the total momentum is conserved in the Coulomb transition. Because of the momentum conservation and the most uniform configuration, the number of the allowed transitions takes the local maximum at the specific filling factors $\nu_0 = 2j/(2j+1)$, $j/(2j-1)$, $j/(2j+1)$, $1/(2j+1)$, $(4j+1)/(2j+1)$, $(3j-1)/(2j-1)$, $(3j+1)/(2j+1)$, $(2j+2)/(2j+1)$ and so on. The transitions produce the binding energy of the electron pair. The larger the number of transitions, the pair energy is lowered. If the filling factor ν deviates from the specific filling factors ν_0 , many Coulomb transitions are forbidden. The forbidden mechanism yields the energy gap at the specific filling factors ν_0 . Thereby, the Hall confinement appears at the specific filling factors. Thus the present theory can explain the FQHE well without any quasi-particle [21]-[26].

The spin-polarizations of FQHE are obtained by V. Kukushkin, K. von Klitzing, and K. Eberl [27]. They clarified the magnetic field dependence of the polarization under fixing the filling factors. Although their experiments are rather old, the polarization curves versus magnetic field give us the very important knowledge. The experimental polarization-curves have the wide plateaus and small shoulders.

There are many spin-arrangements in the most uniform configuration of electrons in the Landau orbitals. These spin-arrangements have the same minimum-expectation-value of H_T . That is to say many electron states with various spin-arrangements are perfectly degenerate. Therefore, we should exactly diagonalize the residual Coulomb interaction. We examine the partial Hamiltonian composed of the strongest and second strongest interactions between electrons. Then we have succeeded to diagonalize the Hamiltonian exactly. The theoretical results are in good agreement with the experimental data. Recently J. K. Jain has written the article [28] and compared the composite fermion (CF) theory [29]-[44] with the Haldane-Halaperin (HH) hierarchy theory [45] [46]. Also he summarized the composite fermion theory and showed the theoretical results on the spin-polarization of FQH states. We compare the polarizations by the CF theory with that by our theory in Section 5.

Next we observe the experimental data [27] in more details. Then we find small shoulders on the curves of the polarization versus magnetic field. The small shoulders appear at the middle between two wide plateaus. This property is similar to the famous feature in the spin-Peierls effect [47]. The spin-Peierls effect is caused by the lattice distortion with the period doubling the unit cell. The sum of spin-energy and distortion-energy (namely total energy) becomes lower than that without distortion. We applied the distortion to the intervals between Landau orbitals in the previous works [48] [49] where the magnitude of distortion was treated to be a fixed value. However the magnitude should be determined by minimizing the total energy in each field strength. Accordingly the magnitude of distortion depends on the field strength. The minimizing of the total energy needs a very complicated program and a long cpu-time. In this article we succeed to make the Mathematica program with

parallel computation. The calculated results show the Peierls instability and the polarization curves are in better agreement with the experimental data than the previous results.

2. Fundamental Properties

A typical quantum Hall device is illustrated in **Figure 1** where the current flows along the x -direction and the magnetic field \mathbf{B} has the z -direction, namely $\mathbf{B} = (0, 0, B)$. In the absence of the Coulomb interaction between electrons, the Hamiltonian of a single electron is given by

$$H_0 = \frac{(\mathbf{p} + e\mathbf{A})^2}{2m^*} + U(y) + W(z), \quad \text{where } \mathbf{A} = (-yB, 0, 0). \quad (1)$$

Therein $W(z)$ is the potential along the z -direction confining electrons to the thin conducting layer. The potential $U(y)$ has large potential difference between both ends, $y=0$ and $y=d$ as in **Figure 2**. In the right hand side of Equation (1), $\mathbf{p} = (p_x, p_y, p_z)$ is the electron momentum and m^* is the effective mass of electron, the value of which differs from material to material. The value of m^* in GaAs is about 0.067 times the free electron mass.

The eigen-value problem of H_0 is solved and the single-electron wave function $\psi_{L,J}$ is expressed as

$$\psi_{L,J}(x, y, z) = \sqrt{\frac{1}{\ell}} \exp(ip_x/\hbar) u_L H_L \left(\sqrt{\frac{m^* \omega}{\hbar}} (y - \alpha_J) \right) \exp\left(-\frac{m^* \omega}{2\hbar} (y - \alpha_J)^2\right) \phi(z) \quad (2)$$

where L the Landau level number, $\phi(z)$ the wave function of the ground state along z -direction, H_L the Hermite polynomial of L -th degree and u_L is the normalization constant. Also α_J is given by

$$\alpha_J = p/(eB) = [2\pi\hbar/(\ell eB)]J, \quad \ell: \text{length of 2D electron system}. \quad (3)$$

The eigenenergy is given by

$$E_{L,J} = \lambda + U(\alpha_J) + \hbar\omega(L + (1/2)), \quad (L = 0, 1, 2, 3, \dots), \quad (4)$$

where λ is the ground state energy along the z -direction and $U(\alpha_J)$ is the potential energy in **Figure 2**.

Next let us consider the many electron system. The total Hamiltonian is given by

$$H_T = \sum_{i=1}^N H_{0,i} + \sum_{i=1}^{N-1} \sum_{j>i}^N \frac{e^2}{4\pi\epsilon\sqrt{(x_i - x_j)^2 + (y_i - y_j)^2 + (z_i - z_j)^2}}, \quad (5a)$$

where N is the total number of electrons and $H_{0,i}$ is the single particle Hamiltonian:

$$H_{0,i} = \frac{(\mathbf{p}_i + e\mathbf{A})^2}{2m^*} + U(y_i) + W(z_i). \quad (5b)$$

The eigenstate of $\sum_{i=1}^N H_{0,i}$ is described by $|\Psi(L_1, \dots, L_N; p_1, \dots, p_N)\rangle$ which is specified by the set of Landau

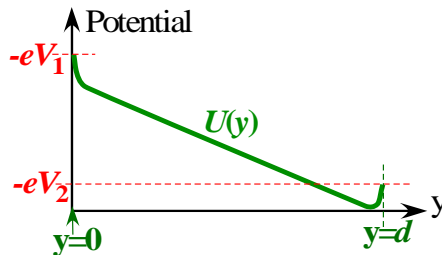


Figure 2. Potential $U(y)$ along the y -direction.

level numbers L_1, L_2, \dots, L_N and momenta p_1, p_2, \dots, p_N . The expectation value of the total Hamiltonian is expressed by $W(L_1, \dots, L_N; p_1, \dots, p_N)$:

$$W(L_1, \dots, L_N; p_1, \dots, p_N) = \sum_{i=1}^N E_{L_i}(p_i) + C(L_1, \dots, L_N; p_1, \dots, p_N), \quad (6)$$

where $C(L_1, \dots, L_N; p_1, \dots, p_N)$ is the expectation value of the Coulomb interaction. Hereafter we call C ‘‘classical Coulomb energy’’. We separate H_T into two parts H_D and H_I . H_D is composed of all diagonal parts and H_I is constructed only by the off-diagonal elements as follows:

$$H_D = \sum_{L_1, \dots, L_N} \sum_{p_1, \dots, p_N} |\Psi(L_1 \dots L_N; p_1, \dots, p_N)\rangle W(L_1 \dots L_N; p_1, \dots, p_N) \langle \Psi(L_1 \dots L_N; p_1, \dots, p_N)|, \quad (7a)$$

$$H_I = H_T - H_D. \quad (7b)$$

Because the Coulomb interaction depends upon only the relative coordinate, the total momentum of the x -direction is conserved in this system as follows:

$$p'_i + p'_j = p_i + p_j \quad (8)$$

where p_i and p_j are the initial momenta and p'_i and p'_j are the final momenta via H_I . All the electrons in the ground state of $\sum_{i=1}^N H_{0,i}$ exist in the lowest Landau levels ($L=0$) for a filling factor $\nu \leq 2$ because

electrons can take up- and down-spin states. If the electrons with the momenta p_1, p_2, \dots, p_N distribute most uniformly in the Landau orbitals, the classical Coulomb energy takes the lowest value. Thereby the many-electron state becomes the ground state of H_D . The momenta p_1, p_2, \dots, p_N are determined by each centre positions $\alpha_{j_1}, \alpha_{j_2}, \dots, \alpha_{j_N}$ namely $p_i = eB \times \alpha_{j_i}$ as in Equation (3). For any filling factor, we can find only one electron-configuration with the minimum energy of H_D . The proof has been done in Ref. [21]. The residual Hamiltonian H_I acts between two electrons. All the initial states with the momenta p_1, p_2 are $|p_1 \uparrow, p_2 \uparrow\rangle$, $|p_1 \uparrow, p_2 \downarrow\rangle$, $|p_1 \downarrow, p_2 \uparrow\rangle$ and $|p_1 \downarrow, p_2 \downarrow\rangle$ where the symbols \uparrow and \downarrow indicate up and down spins, respectively. The final states are $|p'_1 \uparrow, p'_2 \uparrow\rangle$, $|p'_1 \uparrow, p'_2 \downarrow\rangle$, $|p'_1 \downarrow, p'_2 \uparrow\rangle$ and $|p'_1 \downarrow, p'_2 \downarrow\rangle$, where p'_1 and p'_2 are the final momenta via the interaction H_I . Now we consider the Coulomb transitions of only between the degenerate ground states of H_D . The ground states have the most uniform configuration. Therefore the electron-configuration of the final state is equivalent to that of the initial state. So the final momentum set is the same as the initial one. Then we obtain $(p'_1 = p_1, p'_2 = p_2)$ or $(p'_1 = p_2, p'_2 = p_1)$. The case of $(p'_1 = p_1, p'_2 = p_2)$ is removed because the diagonal matrix elements of H_I are zero. Accordingly the final momenta become

$$p'_1 = p_2, \quad p'_2 = p_1. \quad (9)$$

Even if Equation (9) is satisfied, the initial state is identical to the final state for the same spin direction of the two electrons. Therein the transition matrix element is zero. Accordingly non-zero matrix elements are

$$\langle p_2 \uparrow, p_1 \downarrow | H_I | p_1 \uparrow, p_2 \downarrow \rangle \quad (10a)$$

$$\langle p_2 \downarrow, p_1 \uparrow | H_I | p_1 \downarrow, p_2 \uparrow \rangle \quad (10b)$$

where $\langle p_2 \uparrow, p_1 \downarrow | H_I | p_1 \uparrow, p_2 \downarrow \rangle = \langle p_2 \downarrow, p_1 \uparrow | H_I | p_1 \downarrow, p_2 \uparrow \rangle$. We examine following three cases:

$$\text{Case A: } p_1 - p_2 = \pm 2\pi\hbar/\ell \quad \xi = \langle p_2 \uparrow, p_1 \downarrow | H_I | p_1 \uparrow, p_2 \downarrow \rangle \quad (11a)$$

$$\text{Case B: } p_3 - p_4 = \pm 4\pi\hbar/\ell \quad \eta = \langle p_4 \uparrow, p_3 \downarrow | H_I | p_3 \uparrow, p_4 \downarrow \rangle \quad (11b)$$

$$\text{Case C: } p_5 - p_6 = \pm 6\pi\hbar/\ell \quad \varsigma = \langle p_6 \uparrow, p_5 \downarrow | H_I | p_5 \uparrow, p_6 \downarrow \rangle \quad (11c)$$

Figure 3 shows the case A.

This transition is equivalent to the following process: the spin at site 1 flips from up to down, and the spin at site 2 flips from down to up without changing the momenta. Thus the Coulomb transition of the case A is equivalent to a spin exchange process which is described by the interaction $\xi\sigma_1^-\sigma_2^+$. Therein σ^+ is the spin transformation operator from down to up-spin state and σ^- is the adjoint operator of σ^+ . Another Coulomb transition given by Equation (10b) is equivalent to $\xi\sigma_1^+\sigma_2^-$. Accordingly Coulomb transition between sites 1 and 2 is

$$\xi(\sigma_1^-\sigma_2^+ + \sigma_1^+\sigma_2^-) \tag{12}$$

where ξ was already defined by Equation (11a). In this Coulomb transition, the classical Coulomb energy of the initial state is exactly equal to that of the final state.

Next **Figure 4** shows the case B.

Coulomb interactions in Cases B and C are equivalent to the following spin exchange interactions where η and ζ are the coupling constants defined by Equation (11b) and (11c), respectively.

$$\eta(\sigma_3^-\sigma_4^+ + \sigma_3^+\sigma_4^-), \quad \zeta(\sigma_5^-\sigma_6^+ + \sigma_5^+\sigma_6^-) \tag{13}$$

Let us study two examples of $\nu = 2/3$ and $2/5$. The most uniform configuration is in **Figure 5(a)** and **Figure 5(b)**. The spin-states are numbered sequentially from left to right as shown by green color. It is noteworthy that the site-number of spin is different from the orbital number. At the $\nu = 2/3$, the strongest interaction acts between the nearest electron pairs which has the coupling constant ξ . The second strongest interaction has the coupling constant η as shown in **Figure 5(a)**. At $\nu = 2/5$, the strongest and the second strongest interactions have the coupling constants η and ζ as shown in **Figure 5(b)**.

We examine the third strongest interaction at $\nu = 2/3$. Therein another electron is inserted as seen in **Figure 5(a)**. Therefore the interaction between the third nearest electrons becomes weak by the screening effect of the inserted electron in between the pair. At $\nu = 2/5$ the third strongest interaction acts between the electrons placed in the fifth nearest orbitals where another electron is inserted as in **Figure 5(b)**. Therefore the interaction

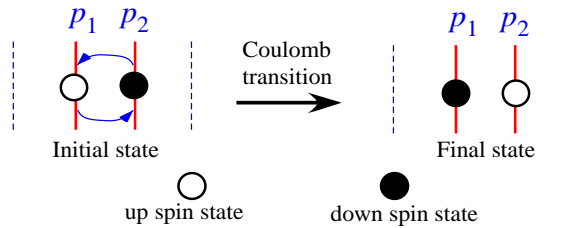


Figure 3. Equivalence of specific Coulomb transition and spin exchange interaction for case A.

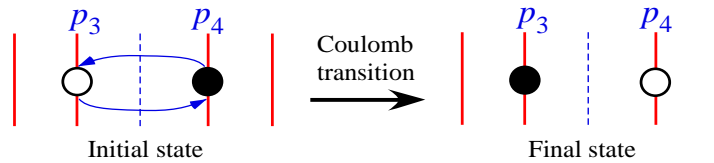


Figure 4. Equivalence of specific Coulomb transition and spin exchange interaction for case B.

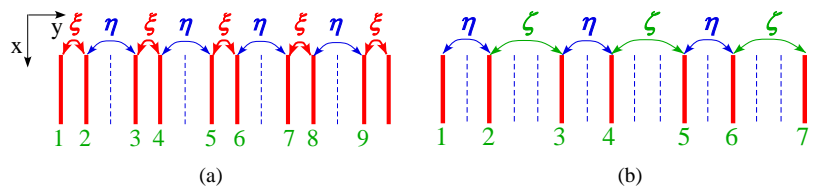


Figure 5. (a) Coulomb transitions at $\nu = 2/3$; (b) Coulomb transitions at $\nu = 2/5$.

becomes weak by the screening effect of the interposing electron. Consequently the most effective interaction is obtained for $\nu = 2/3$ as;

$$H_{\text{effective}} = \sum_{j=1,2,3,\dots} \left[\xi (\sigma_{2j-1}^+ \sigma_{2j}^- + \sigma_{2j-1}^- \sigma_{2j}^+) + \eta (\sigma_{2j}^+ \sigma_{2j+1}^- + \sigma_{2j}^- \sigma_{2j+1}^+) \right]. \quad (14)$$

This Hamiltonian yields the quantum transition between the degenerate ground states. We take account of the Zeeman interaction and get the most effective Hamiltonian as

$$H = \sum_{j=1,2,3,\dots} \left[\xi (\sigma_{2j-1}^+ \sigma_{2j}^- + \sigma_{2j-1}^- \sigma_{2j}^+) + \eta (\sigma_{2j}^+ \sigma_{2j+1}^- + \sigma_{2j}^- \sigma_{2j+1}^+) \right] + \sum_{i=1,2,3,\dots} \mu_B g^* B (1/2) \sigma_i^z \quad (15)$$

where g^* is the effective g -factor, B is the magnetic field, $(1/2)\sigma^z$ is the electron spin operator of the z -direction and μ_B is the Bohr magneton. The Hamiltonians for $\nu = 3/5$ and $\nu = 4/7$ are given by

$$H = \sum_{j=1,2,3,\dots} \left[\xi (\sigma_{3j-2}^+ \sigma_{3j-1}^- + \sigma_{3j-2}^- \sigma_{3j-1}^+) + \eta (\sigma_{3j-1}^+ \sigma_{3j}^- + \sigma_{3j-1}^- \sigma_{3j}^+) + \eta (\sigma_{3j}^+ \sigma_{3j+1}^- + \sigma_{3j}^- \sigma_{3j+1}^+) \right] + \sum_{i=1,2,3,\dots} \mu_B g^* B (1/2) \sigma_i^z, \quad \text{for } \nu = 3/5. \quad (16)$$

$$H = \sum_{j=1,2,3,\dots} \left[\xi (\sigma_{4j-3}^+ \sigma_{4j-2}^- + \sigma_{4j-3}^- \sigma_{4j-2}^+) + \eta (\sigma_{4j-2}^+ \sigma_{4j-1}^- + \sigma_{4j-2}^- \sigma_{4j-1}^+) + \eta (\sigma_{4j-1}^+ \sigma_{4j}^- + \sigma_{4j-1}^- \sigma_{4j}^+) + \eta (\sigma_{4j}^+ \sigma_{4j+1}^- + \sigma_{4j}^- \sigma_{4j+1}^+) \right] + \sum_{i=1,2,3,\dots} \mu_B g^* B (1/2) \sigma_i^z, \quad \text{for } \nu = 4/7. \quad (17)$$

These three Hamiltonians can be exactly diagonalized by using the method of Ref. [50].

3. Diagonalization of the Most Effective Hamiltonian for FQH States

We introduce a new mapping from a spin state to a fermion state. The down-spin state $|\downarrow\rangle$ is mapped to the vacuum state $|0\rangle$ and the up-spin state $|\uparrow\rangle$ is mapped to the fermion state $c^*|0\rangle$ where c^* is the creation operator. Thereby the spin operators σ^+ , σ^- and σ^z are mapped as;

$$\sigma^+ \rightarrow c^*, \quad \sigma^- \rightarrow c, \quad \sigma^z \rightarrow (2c^*c - 1). \quad (18)$$

Many electron states are mapped to the many fermion states where the multiplying order of the creation operators is the same as the order of the up-spins:

$$|\uparrow_1, \uparrow_2, \downarrow_3, \uparrow_4, \downarrow_5, \downarrow_6, \uparrow_7, \downarrow_8, \downarrow_9, \uparrow_{10}, \downarrow_{11}, \uparrow_{12}\rangle \leftrightarrow c_1^* c_2^* c_4^* c_7^* c_{10}^* c_{12}^* |0\rangle \quad (19)$$

where the operators c_i and c_i^* satisfy the anti-commutation relations. The spin operators $\sigma_{2j-1}^+ \sigma_{2j}^-$, $\sigma_{2j-1}^- \sigma_{2j}^+$, $\sigma_{2j}^+ \sigma_{2j+1}^-$ and $\sigma_{2j}^- \sigma_{2j+1}^+$ are mapped to the products of the fermion operators as follows:

$$\sigma_{2j-1}^+ \sigma_{2j}^- \leftrightarrow c_{2j-1}^* c_{2j}, \quad \sigma_{2j-1}^- \sigma_{2j}^+ \leftrightarrow -c_{2j-1} c_{2j}^* \quad (20a)$$

$$\sigma_{2j}^+ \sigma_{2j+1}^- \leftrightarrow c_{2j}^* c_{2j+1}, \quad \sigma_{2j}^- \sigma_{2j+1}^+ \leftrightarrow -c_{2j} c_{2j+1}^* \quad (20b)$$

$$\sigma_i^z \leftrightarrow 2c_i^* c_i - 1. \quad (20c)$$

It has been verified in Ref. [50] that the mapping ((20a), (20b), (20c)) is isomorphic.

Accordingly Hamiltonian Equation (15) is equivalent to the following form:

$$H = \sum_{j=1,2,3,\dots} \left[\xi (c_{2j-1}^* c_{2j} - c_{2j-1} c_{2j}^*) + \eta (c_{2j}^* c_{2j+1} - c_{2j} c_{2j+1}^*) \right] + \sum_{i=1,2,3,\dots} \mu_B g^* B (1/2) (2c_i^* c_i - 1). \quad (21)$$

We can exactly solve the eigen-value problem of H by introducing new operators a_j and b_j :

$$a_j = c_{2j-1}, \quad b_j = c_{2j}, \quad a_j^* = c_{2j-1}^* \quad \text{and} \quad b_j^* = c_{2j}^*, \quad (22)$$

where j is the cell number. Thereby the Hamiltonian (21) becomes

$$H = \sum_{j=1}^J \left[\xi (a_j^* b_j - a_j b_j^*) + \eta (b_j^* a_{j+1} - b_j a_{j+1}^*) \right] + \sum_{j=1}^J \mu_B g^* B (1/2) (2a_j^* a_j + 2b_j^* b_j - 2), \quad (23)$$

where J is the total number of cells given by $J = N/2$ (N is the total number of electrons). We apply a Fourier transformation to Equation (23) and obtain as

$$H = \sum_p \left[\xi (a^*(p)b(p) + b^*(p)a(p)) + \eta (e^{ip} b^*(p)a(p) + e^{-ip} a^*(p)b(p)) \right] + \sum_p \mu_B g^* B (1/2) (2a^*(p)a(p) + 2b^*(p)b(p) - 2), \quad (24)$$

where

$$a_n = \frac{1}{\sqrt{J}} \sum_p e^{ipn} a(p), \quad b_n = \frac{1}{\sqrt{J}} \sum_p e^{ipn} b(p), \quad p = \frac{2\pi}{J} \times \text{integer}, \quad -\pi < p \leq \pi. \quad (25)$$

In Equation (24) the term with one value of p is expressed by the following matrix:

$$\begin{pmatrix} \mu_B g^* B & \xi + \eta e^{-ip} \\ \xi + \eta e^{ip} & \mu_B g^* B \end{pmatrix}. \quad (26)$$

This matrix has two eigen-values $\lambda_1(p)$ and $\lambda_2(p)$ which are given by

$$\lambda_1(p) = \mu_B g^* B - \sqrt{\xi^2 + \eta^2 + 2\xi\eta \cos p}, \quad \lambda_2(p) = \mu_B g^* B + \sqrt{\xi^2 + \eta^2 + 2\xi\eta \cos p}. \quad (27)$$

We introduce new annihilation operators $A_1(p)$ and $A_2(p)$ as follows:

$$A_1(p) = \frac{a(p)}{\sqrt{2}} - \frac{(\xi + \eta e^{-ip})b(p)}{\sqrt{2(\xi^2 + \eta^2 + 2\xi\eta \cos p)}}, \quad A_2(p) = \frac{a(p)}{\sqrt{2}} + \frac{(\xi + \eta e^{-ip})b(p)}{\sqrt{2(\xi^2 + \eta^2 + 2\xi\eta \cos p)}}. \quad (28)$$

Hamiltonian (24) is expressed by making use of $A_1(p)$ and $A_2(p)$ as follows:

$$H = \sum_p (\lambda_1(p) A_1^*(p) A_1(p) + \lambda_2(p) A_2^*(p) A_2(p) - \mu_B g^* B). \quad (29)$$

Thus we have succeeded in diagonalizing the original Hamiltonian (15).

4. Spin-Polarization

The electron-spin polarization γ_e is defined by the thermodynamic mean value as follows:

$$\gamma_e = \frac{1}{N} \left\langle -\sum_{i=1}^N \sigma_i^z \right\rangle = \frac{-1}{N} \left\langle \sum_{j=1}^J (2a_j^* a_j + 2b_j^* b_j - 2) \right\rangle = \frac{-1}{2J} \left\langle \sum_p \left(\sum_{s=1}^2 (2A_s^*(p) A_s(p) - 1) \right) \right\rangle \quad (30)$$

where $\langle \dots \rangle$ is the thermal average and the minus sign comes from the negative charge of electron. All the eigen-states are specified by the set of the numbers $n_s(p) = A_s^*(p) A_s(p)$. The eigen-energy for $n_s(p) = 1$ is $\lambda_s(p)$ and the energy for $n_s(p) = 0$ is zero. The Boltzmann factor is $\exp(-\lambda_s(p)/k_B T)$ for $n_s(p) = 1$ and $\exp(-0/k_B T)$ for $n_s(p) = 0$ where k_B is the Boltzmann constant and T is the temperature. Accordingly, the probability of $n_s(p) = 1$ is $\exp(-\lambda_s(p)/k_B T) / (1 + \exp(-\lambda_s(p)/k_B T))$. Then the thermal average is obtained as follows;

$$\langle 2A_s^*(p) A_s(p) - 1 \rangle = \langle 2n_s(p) - 1 \rangle = \frac{\exp(-\lambda_s(p)/k_B T) - 1}{1 + \exp(-\lambda_s(p)/k_B T)} = -\tanh(\lambda_s(p)/(2k_B T)). \quad (31)$$

Substitution of Equation (31) into Equation (30) gives $\gamma_e = \frac{1}{2J} \sum_p \left(\sum_{s=1}^2 \tanh(\lambda_s(p)/2k_B T) \right)$. Because the momentum interval is extremely small, the electron-spin polarization is expressed by the integration as

$$\gamma_e = \frac{1}{4\pi} \int_{-\pi}^{\pi} dp \left(\sum_{s=1}^2 \tanh(\lambda_s(p)/2k_B T) \right) \quad \text{for } \nu = 2/3. \quad (32)$$

Similarly we obtain the spin-polarization at the filling factors of 3/5 and 4/7 as follows:

$$\gamma_e = \frac{1}{6\pi} \int_{-\pi}^{\pi} dp \left(\sum_{s=1}^3 \tanh(\lambda_s(p)/2k_B T) \right), \quad \gamma_e = \frac{1}{8\pi} \int_{-\pi}^{\pi} dp \left(\sum_{s=1}^4 \tanh(\lambda_s(p)/2k_B T) \right). \quad (33)$$

The calculated results are shown in **Figure 6** which are in good agreement with the experimental data.

5. Comparison between Present Theory and Composite Fermion Theory

J. K. Jain examined the spin-polarization in the CF theory [28]. He wrote as follows: ‘‘For spinful composite fermions, we write $\nu^* = \nu_{\uparrow}^* + \nu_{\downarrow}^*$, where ν_{\uparrow}^* and ν_{\downarrow}^* are the filling factors of up and down spin composite fermions. The possible spin polarizations of the various FQHE states are then predicted by analogy to the IQHE of

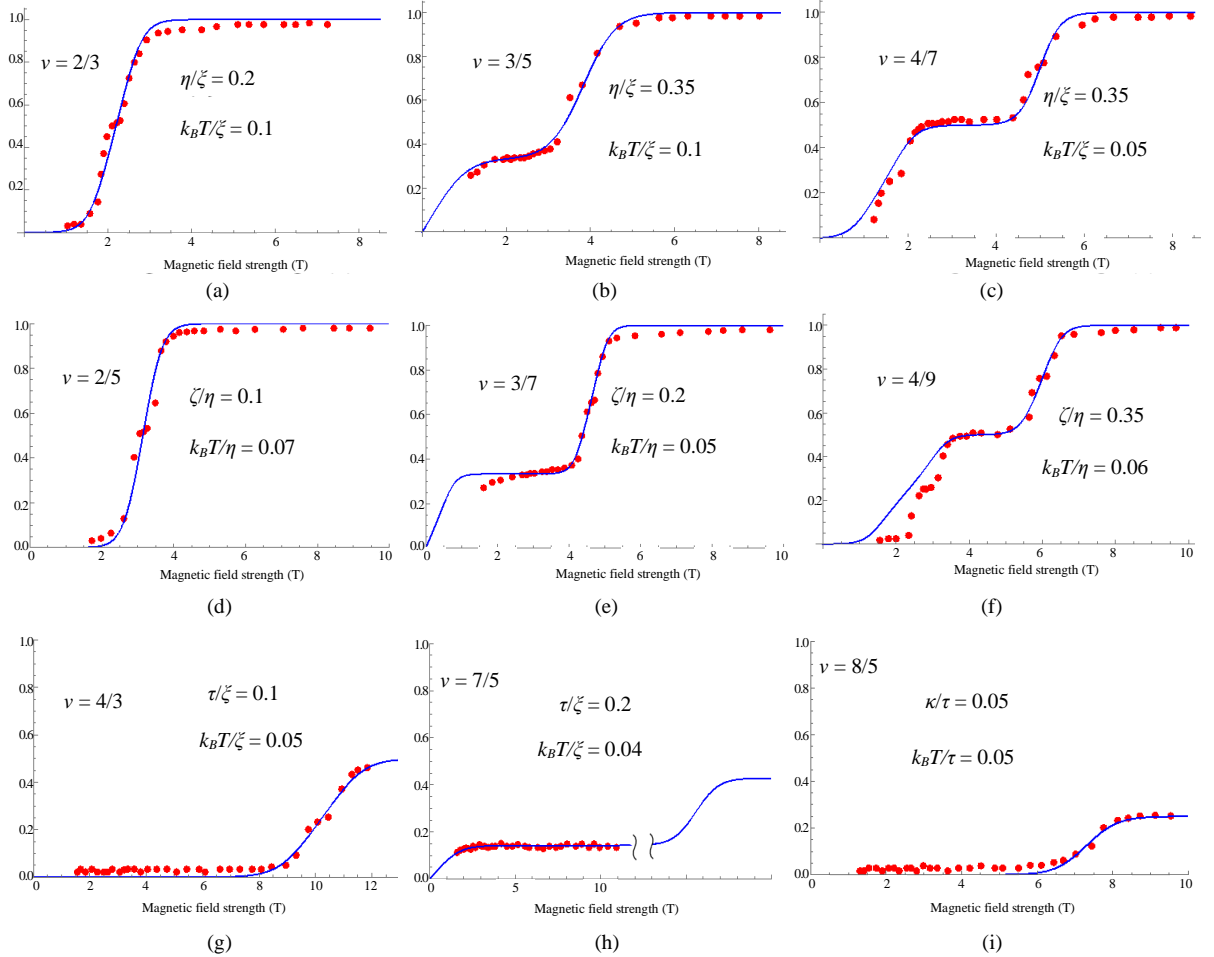


Figure 6. (a) Polarization at $\nu = 2/3$; (b) Polarization at $\nu = 3/5$; (c) Polarization at $\nu = 4/7$; (d) Polarization at $\nu = 2/5$; (e) Polarization at $\nu = 3/7$; (f) Polarization at $\nu = 4/9$; (g) Polarization at $\nu = 4/3$; (h) Polarization at $\nu = 7/5$; (i) Polarization at $\nu = 8/5$. Calculated spin-polarization curves. Red dots are the experimental data [27].

spinful electrons. For example, the 4/7 state maps into $\nu^* = 4$, where we expect, from a model that neglects interaction between composite fermions, a spin singlet state at very low Zeeman energies (with $\nu^* = 2+2$), a partially spin polarized state at intermediate Zeeman energies ($\nu^* = 3+1$), and a fully spin polarized state at large Zeeman energies ($\nu^* = 4+0$)."

The CF cyclotron energy is proportional to \sqrt{B} and the Zeeman energy is proportional to the applied magnetic field B as explained in the article [28]. Then the CF energy ε_{CF} is equal to

$$\varepsilon_{CF}(n \uparrow) = \alpha \left(n - \frac{1}{2} \right) \sqrt{B} + \beta B, \quad \varepsilon_{CF}(n \downarrow) = \alpha \left(n - \frac{1}{2} \right) \sqrt{B} - \beta B \quad (34)$$

where α and β are the coefficients. Therein $n = \nu^* = L^* + 1$ where L^* is the CF Landau level number ($L^* = 0, 1, 2, 3, \dots$). When the filling factor ν of electrons is smaller than $2/3$, ν is expressed by using the CF level number ν^* the number of attached flux quanta $2p$ as follows:

$$\nu = \nu^* / (2p\nu^* \pm 1). \quad (35)$$

When the sign in the denominator is plus, the effective magnetic field is parallel to the applied magnetic field. So the coefficient β becomes positive. On the other hand the effective magnetic field has opposite direction against the applied field for the minus sign in Equation (35). Then β is negative. We obtain the sum of the CF cyclotron energy and the Zeeman energy for various CF levels and CF spins. The results are shown in Figure 7 where we find the crossing points between the energies for spin-up and down states. The ratio of the field strengths at the crossing points is 1:4:9:16 and so on. For an example $\nu = 4/7$ the composite fermions occupy the lowest four levels which are indicated by the bold curves as in Figure 8(a). The ratio of the strength B_1 , B_2 and B_3 is 1:4:9. Accordingly the spin-polarization depends on the magnetic field strength at zero temperature as in Figure 8(b).

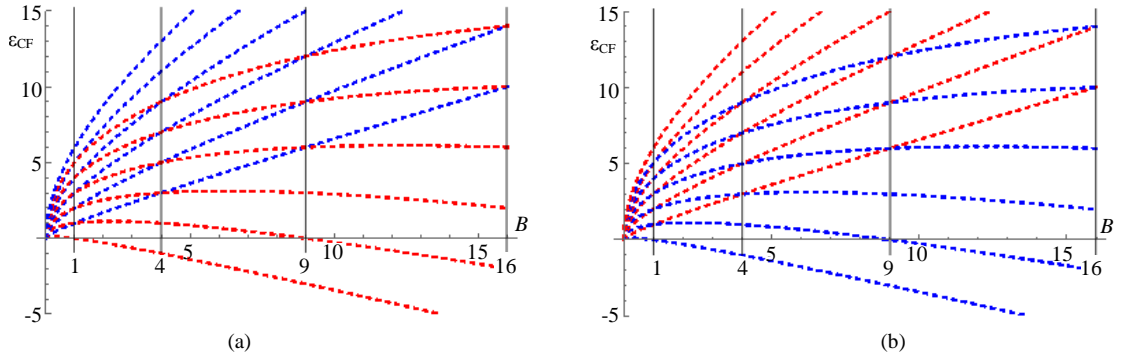


Figure 7. (a) Energy of CF for $\nu^*/(2p\nu^* + 1)$; (b) Energy of CF for $\nu^*/(2p\nu^* - 1)$; Blue dashed curves for up-spin CF, red for down spin CF. The axes are drawn with arbitrary scale.

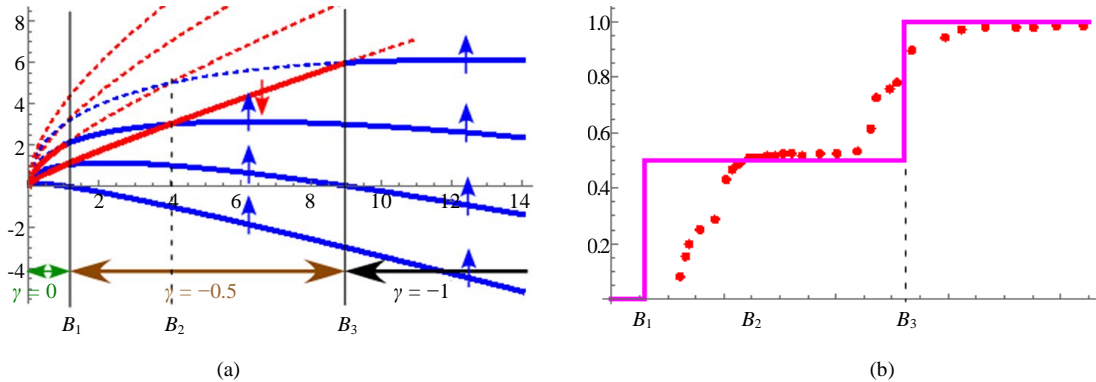


Figure 8. (a) Ground state in CF theory at $\nu = 4/7$; (b) Polarization of CF state at $\nu = 4/7$.

It is noteworthy that the effective field is opposite against the applied field at $\nu = 4/7$. Let us compare the spin-polarization of the CF theory with that of the present theory at a finite temperature. **Figure 9(a)** shows the CF result and **Figure 9(b)** our result at $\nu = 4/7$. The CF result is different from the experimental data [27] in the low magnetic field region.

Similarly we compare the CF result with our result at $\nu = 3/5$ in **Figure 10(a)** and **Figure 10(b)**. Our theory employs only the normal electrons without any quasi-particle. The partial Hamiltonian with the strongest and second strongest interactions is diagonalized exactly. Then the results are in good agreement with the experimental data. On the other hand the results via the CF theory deviate from the experimental data. Moreover the direction of CF polarization at $\nu = 2/3, 3/5, 4/7$, etc is opposite against that of normal electrons because the effective magnetic field is opposite against the applied field. But the direction of CF polarization at $\nu = 1/3, 2/5, 3/7, 4/9$, etc is the same as that of normal electrons. So it is necessary to measure the direction of the polarization especially at $\nu = 2/3, 3/5, 4/7$.

6. Spin Peierls Instability in FQH States

When the experimental data [27] of the spin polarization is carefully observed, we can find a small shoulder in the middle of two wide plateaus. This structure resembles the famous mechanism “spin Peierls effect”. R. E. Peierls studied an electron system in a one dimensional crystal and considered the lattice distortion with the period doubling the unit cell. This distortion produces new band gaps and the energy becomes lower than without the distortion. The effect is called spin Peierls effect [47].

We apply a new distortion for the intervals between Landau orbitals. We change the distance between orbitals in the first unit-configuration longer, that in the second unit-configuration shorter and so on. We call it “interval modulation”. As an example $\nu = 2/3$, we illustrate the modulation in **Figure 11** where we obtain new four

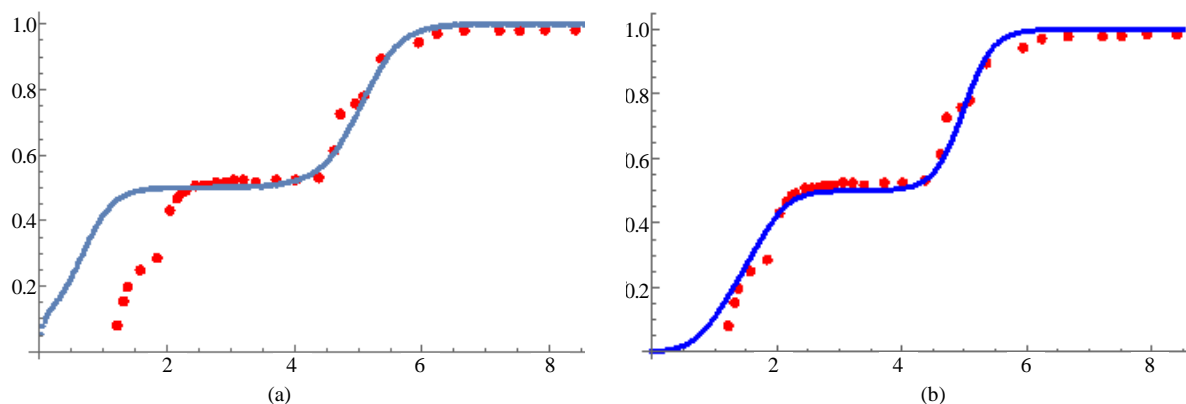


Figure 9. (a) CF result at $\nu = 4/7$ in a finite temperature; (b) Our theory at $\nu = 4/7$.

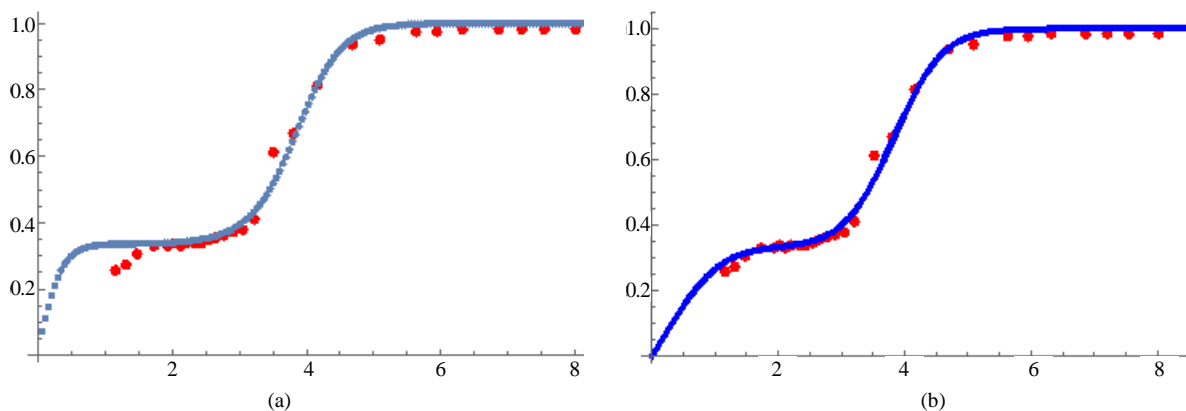


Figure 10. (a) CF result at $\nu = 3/5$; (b) Our result at $\nu = 3/5$.

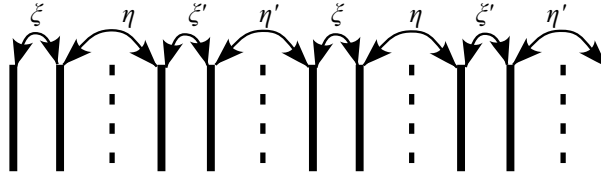


Figure 11. Coupling constants of interactions caused by distortion with double period.

coupling constants ξ , ξ' , η and η' . The value of ξ' is larger than ξ because the ξ' interaction path is shorter than that of ξ . Also, $\eta' > \eta$ holds.

We express the distance between nearest Landau orbitals by the symbol r_0 in non-distortion case. The distance becomes $r_0 + d$ for an odd cell number and the other one becomes $r_0 - d$ for an even cell number. Then, the classical Coulomb energy W increases. The increasing value per electron is proportional to d^2 as $\Delta W/N = f_c (d/r_0)^2$ where f_c is the constant parameter. We next examine d -dependence of ξ and ξ' . When $d > 0$, the coupling constant ξ is weaker than ξ' because the ξ interaction path is longer than that of ξ' . When $d < 0$, ξ is stronger than ξ' because the ξ interaction path is shorter than that of ξ' . So the d -dependence in ξ and ξ' is given by

$$\xi = \xi_0 - f_\xi (d/r_0), \quad \xi' = \xi_0 + f_\xi (d/r_0) \quad (36)$$

where ξ_0 is the coupling constant for the non-distortion case and f_ξ is the proportionality constant. A new dimensionless quantity t is introduced as follows

$$t = (f_\xi / \xi_0) (d/r_0). \quad (37)$$

Thereby the coupling constants ξ and ξ' is expressed as

$$\xi = \xi_0 (1-t), \quad \xi' = \xi_0 (1+t). \quad (38)$$

The increasing classical Coulomb-energy ΔW is also described by the distortion parameter t as:

$$\Delta W/N = \xi_0 C t^2 \quad (39)$$

where C is the dimensionless coefficient as $C = \xi_0 f_c / f_\xi^2$.

We calculate the total energy produced by this distortion. Use of the isomorphic mapping namely Equations ((20a), (20b), (20c)) give the spin exchange Hamiltonian for $\nu = 2/3$:

$$H = \sum_{j=1,2,3,\dots} \left[\xi (c_{4j-3}^* c_{4j-2} - c_{4j-3} c_{4j-2}^*) + \eta (c_{4j-2}^* c_{4j-1} - c_{4j-2} c_{4j-1}^*) \right] \\ + \sum_{j=1,2,3,\dots} \left[\xi' (c_{4j-1}^* c_{4j} - c_{4j-1} c_{4j}^*) + \eta' (c_{4j}^* c_{4j+1} - c_{4j} c_{4j+1}^*) \right] + \sum_{i=1,2,3,\dots} \mu_B g^* B (1/2) (2c_i^* c_i - 1). \quad (40)$$

We introduce new operators $a_{1,j}$, $a_{2,j}$, $a_{3,j}$, $a_{4,j}$ and make the Fourier transformation of the operators:

$$a_{1,j} = c_{4j-3}, \quad a_{2,j} = c_{4j-2}, \quad a_{3,j} = c_{4j-1}, \quad a_{4,j} = c_{4j} \quad (41)$$

$$a_{1,j} = \frac{1}{\sqrt{J}} \sum_p e^{ipj} a_1(p), \quad a_{2,j} = \frac{1}{\sqrt{J}} \sum_p e^{ipj} a_2(p), \quad a_{3,j} = \frac{1}{\sqrt{J}} \sum_p e^{ipj} a_3(p), \quad a_{4,j} = \frac{1}{\sqrt{J}} \sum_p e^{ipj} a_4(p) \quad (42)$$

where J is the total cell number namely $J = N/4$, and $p = (2\pi/J) \times \text{integer}$ ($-\pi < p \leq \pi$). Substitution of Equations (41) and (42) into Equation (40) yields

$$H = \sum_p \left[\xi (a_1^*(p) a_2(p) + a_2^*(p) a_1(p)) + \eta (a_2^*(p) a_3(p) + a_3^*(p) a_2(p)) + \xi' (a_3^*(p) a_4(p) + a_4^*(p) a_3(p)) \right. \\ \left. + \eta' (e^{ip} a_4^*(p) a_1(p) + e^{-ip} a_1^*(p) a_4(p)) \right] \\ + \sum_p \mu_B g^* B (1/2) (2(a_1^*(p) a_1(p) + a_2^*(p) a_2(p) + a_3^*(p) a_3(p) + a_4^*(p) a_4(p)) - 4). \quad (43)$$

For each value of p , the right hand side of Equation (43) is expressed by the following matrix M :

$$M = \begin{pmatrix} \mu_B g^* B & \xi & 0 & \eta' e^{-ip} \\ \xi & \mu_B g^* B & \eta & 0 \\ 0 & \eta & \mu_B g^* B & \xi' \\ \eta' e^{ip} & 0 & \xi' & \mu_B g^* B \end{pmatrix}. \quad (44)$$

Here we assume that the ratio ξ'/ξ is almost equal to the ratio η'/η because the interval modulation gives the same effects to ξ and η . Then Equation (38) yields the following ratios:

$$\beta = \xi'/\xi = \eta'/\eta = (1+t)/(1-t) \quad (45a)$$

$$\alpha = \eta/\xi = \eta'/\xi' = \eta_0/\xi_0. \quad (45b)$$

Four eigen-values of M are expressed by the symbols $\lambda_1(p)$, $\lambda_2(p)$, $\lambda_3(p)$ and $\lambda_4(p)$ ($\lambda_1 \leq \lambda_2 \leq \lambda_3 \leq \lambda_4$). The eigen-energies is obtained by using Equations (45a) and (45b):

$$\begin{aligned} \lambda_1(p) &= \mu_B g^* B - \sqrt{\frac{1}{2} \left((1+\alpha^2)(\xi^2 + \xi'^2) + \sqrt{(1+\alpha^2)^2 (\xi^2 + \xi'^2)^2 - 4((1+\alpha^4)\xi^2 \xi'^2 - 2\alpha^2 \xi^2 \xi'^2 \cos p)} \right)}, \\ \lambda_2(p) &= \mu_B g^* B - \sqrt{\frac{1}{2} \left((1+\alpha^2)(\xi^2 + \xi'^2) - \sqrt{(1+\alpha^2)^2 (\xi^2 + \xi'^2)^2 - 4((1+\alpha^4)\xi^2 \xi'^2 - 2\alpha^2 \xi^2 \xi'^2 \cos p)} \right)}, \\ \lambda_3(p) &= \mu_B g^* B + \sqrt{\frac{1}{2} \left((1+\alpha^2)(\xi^2 + \xi'^2) - \sqrt{(1+\alpha^2)^2 (\xi^2 + \xi'^2)^2 - 4((1+\alpha^4)\xi^2 \xi'^2 - 2\alpha^2 \xi^2 \xi'^2 \cos p)} \right)}, \\ \lambda_4(p) &= \mu_B g^* B + \sqrt{\frac{1}{2} \left((1+\alpha^2)(\xi^2 + \xi'^2) + \sqrt{(1+\alpha^2)^2 (\xi^2 + \xi'^2)^2 - 4((1+\alpha^4)\xi^2 \xi'^2 - 2\alpha^2 \xi^2 \xi'^2 \cos p)} \right)}. \end{aligned} \quad (46)$$

Then the diagonal form of the Hamiltonian (43) is expressed by the eigen-energies $\lambda_1, \lambda_2, \lambda_3, \lambda_4$ as:

$$H = \sum_p \left(\lambda_1(p) A_1^*(p) A_1(p) + \lambda_2(p) A_2^*(p) A_2(p) + \lambda_3(p) A_3^*(p) A_3(p) + \lambda_4(p) A_4^*(p) A_4(p) - 2\mu_B g^* B \right). \quad (47)$$

The thermal average $\langle A_s^*(p) A_s(p) \rangle$ is expressed by the eigen-energies as derived in Equation (31).

$$\langle A_s^*(p) A_s(p) \rangle = \frac{\exp(-\lambda_s(p)/k_B T)}{1 + \exp(-\lambda_s(p)/k_B T)} = \frac{1}{2} \left(1 - \tanh(\lambda_s(p)/(2k_B T)) \right) \quad (48)$$

Then the spin exchange energy is

$$\langle H \rangle = \sum_p \left[\left\{ \sum_{s=1}^4 \left(\lambda_s(p) \frac{1}{2} \left(1 - \tanh(\lambda_s(p)/(2k_B T)) \right) \right) \right\} - 2\mu_B g^* B \right]. \quad (49)$$

We can replace the summation in Equation (49) by the integration because the total number of electrons is a macroscopic value.

$$\frac{\langle H \rangle}{N} = \frac{1}{4} \times \frac{1}{2\pi} \int_{p=0}^{2\pi} \left[\left\{ \sum_{s=1}^4 \left(\lambda_s(p) \frac{1}{2} \left(1 - \tanh(\lambda_s(p)/2k_B T) \right) \right) - 2\mu_B g^* B \right\} \right] dp \quad (50)$$

The total energy per electron is the sum of the classical Coulomb energy and the spin energy as

$$\Delta E_{\text{Total}}/N = (\Delta W/N) + \Delta(\langle H \rangle/N). \quad (51)$$

Figure 12 shows the classical Coulomb energy for the parameter $C = 0.5$ in Equation (39) by the dashed black curve. Also the spin-exchange energy $\Delta(\langle H \rangle/N)$ at $B = 2.2[\text{T}]$ is expressed by the red dashed curve.

The blue curve indicates the total energy $\Delta E_{\text{Total}}/N$ which has a minimum value at a non-zero t . Thus the interval modulation occurs actually.

The $\nu = 3/5$ state are illustrated in **Figure 13**. These coupling constants yield the $\nu = 3/5$ Hamiltonian which has the six eigen-values $\lambda_1(p)$, $\lambda_2(p)$, $\lambda_3(p)$, $\lambda_4(p)$, $\lambda_5(p)$ and $\lambda_6(p)$. Also we obtain the eight eigen-values for the $\nu = 4/7$ state.

7. Spin Polarization with Interval Modulation

We have obtained the diagonal forms of the Hamiltonians which have the Peierls instability. The spin-polarization γ_e is given by the integration as:

$$\gamma_e = \frac{1}{8\pi} \int_{-\pi}^{\pi} dp \left(\sum_{s=1}^4 \tanh(\lambda_s(p)/2k_B T) \right) \quad \text{for } \nu = 2/3 \quad (52a)$$

$$\gamma_e = \frac{1}{12\pi} \int_{-\pi}^{\pi} dp \left(\sum_{s=1}^6 \tanh(\lambda_s(p)/2k_B T) \right) \quad \text{for } \nu = 3/5 \quad (52b)$$

$$\gamma_e = \frac{1}{16\pi} \int_{-\pi}^{\pi} dp \left(\sum_{s=1}^8 \tanh(\lambda_s(p)/2k_B T) \right) \quad \text{for } \nu = 4/7 \quad (52c)$$

We numerically calculate the spin-polarization γ_e by the following method: First we search the distortion t with the minimum total energy for each magnetic field. The searching process is shown in **Figure 12** at $\nu = 2/3$ and $B = 2.2[\text{T}]$. Thus we get the distortion value t and the eigen-energies $\lambda_s(p)$ for each magnetic field strength. The eigen-energies are substituted into Equations (52a), (52b) and (52c) and then the spin-polarization is obtained. The theoretical curve is shown in **Figure 14**.

Therein we use the parameter-values $\alpha = \eta/\xi = \eta'/\xi' = 0.2$, $(k_B T/\xi_0) = 0.1$ and $C = 0.5$ for $\nu = 2/3$. At $\nu = 3/5$, the parameter-values are $\alpha = 0.35$, $(k_B T/\xi_0) = 0.1$ and $C = 0.5$. At $\nu = 4/7$, the parameter-values are $\alpha = 0.35$, $(k_B T/\xi_0) = 0.05$ and $C = 0.5$. The calculated results are in good agreement with the experimental data as shown in **Figure 14**.

Next we examine the $\nu = 2/5$, $\nu = 3/7$, and $\nu = 4/9$ states with the interval modulation. For an example of $\nu = 2/5$ the most uniform electron-configuration is illustrated in **Figure 15**.

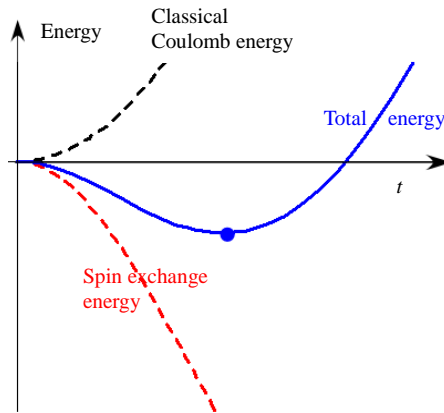


Figure 12. Total energy versus distortion parameter t .

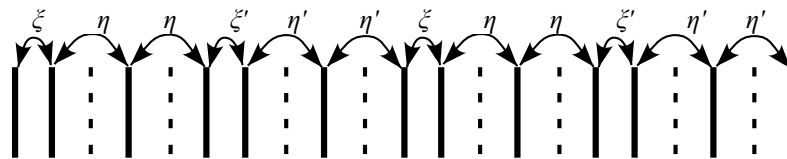


Figure 13. Coupling constants for $\nu = 3/5$.

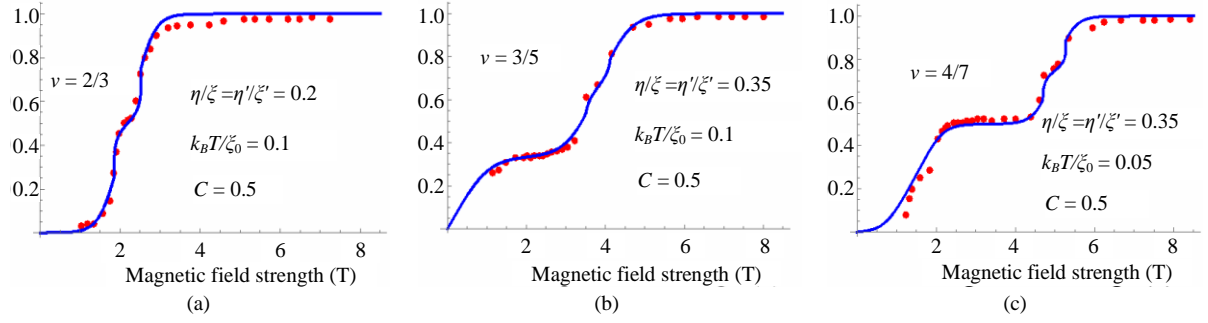


Figure 14. Polarization of the present theory (red dots indicate the experimental data [27]).

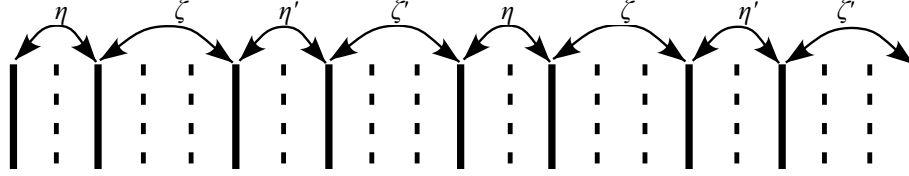


Figure 15. Coupling constants for $\nu = 2/5$.

The interval modulation yields the coupling constants η , η' , ζ and ζ' as follows:

$$\eta = \eta_0(1-t), \quad \eta' = \eta_0(1+t), \quad \zeta = \zeta_0(1-t), \quad \zeta' = \zeta_0(1+t). \quad (53)$$

The ratios between the coupling constants satisfy the following relations;

$$\zeta/\eta = \zeta'/\eta' = \zeta_0/\eta_0, \quad \eta'/\eta = \zeta'/\zeta = (1+t)/(1-t). \quad (54)$$

We express the spin-exchange and classical Coulomb energies by the same parameter η_0 as

$$\Delta W/N = \eta_0 D t^2. \quad (55)$$

Therein the coefficient D is newly introduced. Using the eigen-values of the matrices, we numerically calculate the spin-polarization curves which are shown in **Figure 16**.

Next we examine the spin-polarization at $\nu = 4/3$, $7/5$, and $8/5$. The most uniform electron-configuration and the coupling constants are shown in **Figure 17** for two examples of $\nu = 4/3$ and $8/5$.

The coupling constants at $\nu = 8/5$ are τ , κ , τ' , κ' as in **Figure 17**. Accordingly the coupling constants and the classical Coulomb energy are re-expressed by using τ_0 as follows:

$$\tau = \tau_0(1-t), \quad \tau' = \tau_0(1+t), \quad \kappa = \kappa_0(1-t), \quad \kappa' = \kappa_0(1+t) \quad (56)$$

$$\Delta W/N = \tau_0 E t^2 \quad (57)$$

where the new coefficient E takes the value $E = 1.5$ for $\nu = 8/5$. The doubly occupied orbitals are indicated by the double lines where the electron pair has no polarization because of cancellation by up and down spins. The spin exchange forces act between electrons placed in singly occupied orbitals of **Figure 17**. That is to say two electrons per four electrons have no polarization at $\nu = 4/3$, four electrons per seven electrons have no polarization at $\nu = 7/5$ and also six electrons per eight electrons have no polarization at $\nu = 8/5$. We numerically calculate the spin-polarization curves as in **Figure 18**.

Thus the small shoulders are caused by the Peierls instability as seen in **Figure 14**, **Figure 16** and **Figure 18**.

The theoretical results are in good agreement with the experimental data.

8. Discussion

In Jain's scheme the $\nu = 4/5$ ($\nu = 6/5$) state is assigned to the superposition of the IQH state with $\nu = 1$ and the composite hole (fermion) state with $\nu = -1/5$ ($\nu = 1/5$) as mentioned in the Ref. [28]. Accordingly polarization behaviors of the two states resemble that of the $\nu = 1/5$ state in the CF theory. On the other hand the

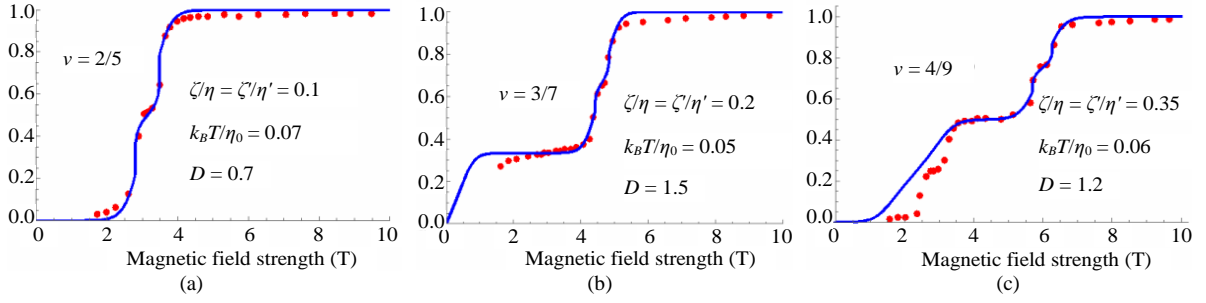


Figure 16. Spin-polarization for $\nu = 2/5, 3/7, 4/9$ (red dots are experimental data [27]).

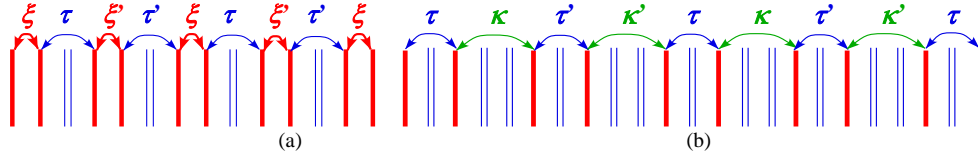


Figure 17. Coupling constants at $\nu = 4/3$ and $8/5$. Double-line indicates a Landau orbital occupied by electron pair with up and down spins.

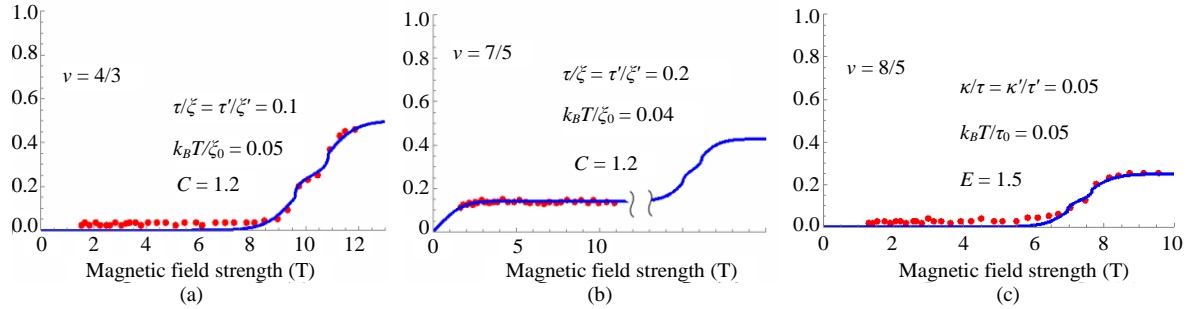


Figure 18. Spin-polarization for $\nu = 4/3, 7/5$ and $8/5$ (red dots are the experimental data [27]).

polarization behavior of the present theory at $\nu = 4/5$ resembles that at $\nu = 4/7$ because there are four electrons per unit-configuration in both $\nu = 4/5$ and $4/7$ states. We can calculate the polarization versus magnetic field at $\nu = 4/5$ and $6/5$ by diagonalizing the 4×4 matrix (8×8 matrix for considering of spin Pierls effect) as mentioned in Sections 3-7. Accordingly the theoretical predictions at $\nu = 4/5$ and $6/5$ are quite different between the CF theory and our theory. The present author cannot find the experimental curves of the polarization versus magnetic field at $\nu = 4/5$ and $6/5$. If there are already raw data in experiments, it is preferable to make the curve of the polarization versus magnetic field.

We cannot also find the experimental data of the spin direction. The effective magnetic field in the CF theory is opposite against the applied field for the filling factor $\nu = \nu^*/(2p\nu^* - 1)$. So it is important to measure the direction of the polarization at the filling factors $\nu = 2/3, 3/5, 4/7$, etc.

9. Conclusions

We have examined the 2D electron system with the total Hamiltonian composed of the three kinds of interactions namely the strong magnetic field interaction, the Coulomb interaction between electrons and the electric potential produced by the Hall voltage. We have found only one electron configuration in the Landau orbitals with the minimum expectation value of the total Hamiltonian for arbitrary filling factor. Up and down spins coexist when the magnetic field is weak. Accordingly there are various spin-arrangements with the same electron configuration. The many states with different spin-arrangements have the same Coulomb energy namely exactly degenerate states. Accordingly we must diagonalize the partial Hamiltonian between the degenerate ground states.

The total momentum along the x -direction conserves via the Coulomb interactions. When the electron 1 placed in the Landau orbital A transfers to the orbital B, the electron 2 placed in the orbital B should transfer to the orbital A because of the total momentum conservation and the relation between momentum and orbital position. We have found the most effective Hamiltonian which is composed of the strongest and second strongest Coulomb interactions. Then we have succeeded to diagonalize the most effective Hamiltonian exactly. The calculated eigen-energies yield the theoretical value of the polarization which has reproduced the wide plateaus on the spin polarization curves. Furthermore we have applied the interval modulation between Landau orbitals and have solved the eigen-equation of the new Hamiltonian. The total energy decreases by the interval modulation. So the modulation appears actually. Thereby the calculated polarization curves have the small shoulders in addition to the wide plateaus. The theoretical results are in good agreement with the experimental data [27].

Acknowledgements

The author expresses his heartfelt appreciation for encouragement of Professor Masayuki Hagiwara, Professor Koichi Katsumata, Professor Hidenobu Hori, Professor Yasuyuki Kitano and Professor Takeji Kebukawa.

References

- [1] von Klitzing, K., Landwehr, G. and Dorda, G. (1974) *Solid State Communications*, **14**, 387-393. [http://dx.doi.org/10.1016/0038-1098\(74\)90566-3](http://dx.doi.org/10.1016/0038-1098(74)90566-3)
- [2] Ando, T., Matsumoto, Y. and Uemura, Y. (1975) *Journal of the Physical Society of Japan*, **39**, 279-288. <http://dx.doi.org/10.1143/JPSJ.39.279>
- [3] von Klitzing, K., Dorda, G. and Pepper, M. (1980) *Physical Review Letters*, **45**, 494. <http://dx.doi.org/10.1103/PhysRevLett.45.494>
- [4] Tsui, D.C. and Gossard, A.C. (1981) *Applied Physics Letters*, **37**, 550. <http://dx.doi.org/10.1063/1.92408>
- [5] Tsui, D.C., Stormer, H.L. and Gossard, A.C. (1982) *Physical Review B*, **25**, 1405. <http://dx.doi.org/10.1103/PhysRevB.25.1405>
- [6] Tsui, D.C., Stormer, H.L. and Gossard, A.C. (1982) *Physical Review Letters*, **48**, 1559. <http://dx.doi.org/10.1103/PhysRevLett.48.1559>
- [7] Laughlin, R.B. (1983) *Physical Review B*, **27**, 3383. <http://dx.doi.org/10.1103/PhysRevB.27.3383>
- [8] Laughlin, R.B. (1983) *Physical Review Letters*, **50**, 1395. <http://dx.doi.org/10.1103/PhysRevLett.50.1395>
- [9] Girvin, S.M. (1984) *Physical Review B*, **29**, 6012. <http://dx.doi.org/10.1103/PhysRevB.29.6012>
- [10] von Klitzing, K. (1986) *Reviews of Modern Physics*, **58**, 519-531. <http://dx.doi.org/10.1103/RevModPhys.58.519>
- [11] von Klitzing, K. (1993) Nobel Lecture, December 9, 1985, The Quantized Hall Effect. In: Frängsmyr, T. and Ekspong, G., Eds., *Nobel Lectures, Physics 1981-1990*, World Scientific, Singapore, 317.
- [12] Willet, R., Eisenstein, J.P., Stormer, H.L., Tsui, D.C., Gossard, A.C. and English, J.H. (1987) *Physical Review Letters*, **59**, 1776-1779. <http://dx.doi.org/10.1103/PhysRevLett.59.1776>
- [13] Eisenstein, J.P. and Stormer, H.L. (1990) *Science*, **248**, 1510-1516. <http://dx.doi.org/10.1126/science.248.4962.1510>
- [14] Stormer, H.L. (2002) Nobel Lecture, December 8, 1998, The Fractional Quantum Hall Effect. In: Ekspong, G., Ed., *Nobel Lectures, Physics 1996-2000*, World Scientific, Singapore, 295-325.
- [15] Pan, W., Stormer, H.L., Tsui, D.C., Pfeiffer, L.N., Baldwin, K.W. and West, K.W. (2002) *Physical Review Letters*, **88**, Article ID: 176802. <http://dx.doi.org/10.1103/PhysRevLett.88.176802>
- [16] Pan, W., Stormer, H.L., Tsui, D.C., Pfeiffer, L.N., Baldwin, K.W. and West, K.W. (2003) *Physical Review Letters*, **90**, Article ID: 016801. <http://dx.doi.org/10.1103/PhysRevLett.90.016801>
- [17] Novoselov, K.S., Jiang, Z., Zhang, Y., Morozov, S.V., Stormer, H.L., Zeitler, U., Maan, J.C., Boebinger, G.S., Kim, P. and Geim, A.K. (2007) *Science*, **315**, 1379. <http://dx.doi.org/10.1126/science.1137201>
- [18] Jeckelmann, B. and Jeanneret, B. (2001) *Reports on Progress in Physics*, **64**, 1603-1655. <http://dx.doi.org/10.1088/0034-4885/64/12/201>
- [19] Tao, R. and Thouless, D.J. (1983) *Physical Review B*, **28**, 1142-1144. <http://dx.doi.org/10.1103/PhysRevB.28.1142>
- [20] Tao, R. (1984) *Physical Review B*, **29**, 636-644. <http://dx.doi.org/10.1103/PhysRevB.29.636>
- [21] Sasaki, S. (2012) *Advances in Condensed Matter Physics*, **2012**, Article ID: 281371. <http://dx.doi.org/10.1155/2012/281371>

- [22] Sasaki, S. (2000) *Physica B: Condensed Matter*, **281-282**, 838-839. [http://dx.doi.org/10.1016/S0921-4526\(99\)00840-6](http://dx.doi.org/10.1016/S0921-4526(99)00840-6)
- [23] Sasaki, S. (2011) Binding Energy, Polarization of Fractional Quantum Hall State. *Proceedings of the 25th International Conference on the Physics of Semiconductors*, Part II, Osaka, 17-22 September 2000, 925-926.
- [24] Sasaki, S. (2003) *Surface Science*, **532-535**, 567-575. [http://dx.doi.org/10.1016/S0039-6028\(03\)00091-8](http://dx.doi.org/10.1016/S0039-6028(03)00091-8)
- [25] Sasaki, S. (2008) *Journal of Physics: Conference Series*, **100**, Article ID: 042021. <http://dx.doi.org/10.1088/1742-6596/100/4/042021>
- [26] Sasaki, S. (2014) *Condensed Matter Physics*, **2014**, Article ID: 468130.
- [27] Kukushkin, I.V., von Klitzing, K. and Eberl, K. (1999) *Physical Review Letters*, **82**, 3665.
- [28] Jain, J.K. (2014) *Indian Journal of Physics*, **88**, 915-929. <http://dx.doi.org/10.1007/s12648-014-0491-9>
- [29] Jain, J.K. (1989) *Physical Review Letters*, **63**, 199-202. <http://dx.doi.org/10.1103/PhysRevLett.63.199>
- [30] Lopez, A. and Fradkin, E. (1991) *Physical Review B*, **44**, 5246-5262. <http://dx.doi.org/10.1103/PhysRevB.44.5246>
- [31] Halperin, B.I., Lee, P.A. and Read, N. (1993) *Physical Review B*, **47**, 7312-7343. <http://dx.doi.org/10.1103/PhysRevB.47.7312>
- [32] Schwarzschild, B. (1993) *Physics Today*, **46**, 17-20.
- [33] Du, R.R., Stormer, H.L., Tsui, D.C., Pfeiffer, L.N. and West, K.W. (1993) *Physical Review Letters*, **70**, 2944-2947. <http://dx.doi.org/10.1103/PhysRevLett.70.2944>
- [34] Jain, J.K. (2007) *Composite Fermions*. Cambridge University Press, New York. <http://dx.doi.org/10.1017/CBO9780511607561>
- [35] Das Sarma, S. (1996) Localization, Metal-Insulator Transitions, and Quantum Hall Effect. In: Das Sarma, S. and Pinczuk, A., Eds., *Perspectives in Quantum Hall Effects: Novel Quantum Liquids in Low-Dimensional Semiconductor Structures*, Wiley, New York, 1-36. <http://dx.doi.org/10.1002/9783527617258.ch1>
- [36] Jain, J.K. and Kamilla, R.K. (1998) Composite Fermions: Particles of the Lowest Landau Level. In: Heinonen, O., Ed., *Composite Fermions: A Unified View of the Quantum Hall Regime*, World Scientific, New York, 1-90. http://dx.doi.org/10.1142/9789812815989_0001
- [37] Halperin, B.I. (2004) Fermion Chern-Simons Theory and the Unquantized Quantum Hall Effect. In: Das Sarma, S. and Pinczuk, A., Eds., *Perspectives in Quantum Hall Effects: Novel Quantum Liquids in Low-Dimensional Semiconductor Structures*, Wiley, New York, 225-263.
- [38] Stormer, H.L. and Tsui, D.C. (1996) Composite Fermions in the Fractional Quantum Hall Effect. In: Das Sarma, S. and Pinczuk, A., Eds., *Perspectives in Quantum Hall Effects: Novel Quantum Liquids in Low-Dimensional Semiconductor Structures*, Wiley, New York, 285-421. <http://dx.doi.org/10.1002/9783527617258.ch10>
- [39] Lopez, A. and Fradkin, E. (1998) Fermionic Chern-Simons Field Theory for the Fractional Quantum Hall Effect. In: Heinonen, O., Ed., *Composite Fermions: A Unified View of the Quantum Hall Regime*, World Scientific, New York, 195-253. http://dx.doi.org/10.1142/9789812815989_0003
- [40] Simon, S.H. (1998) The Chern-Simons Fermi Liquid Description of Fractional Quantum Hall States. In: Heinonen, O., Ed., *Composite Fermions: A Unified View of the Quantum Hall Regime*, World Scientific, New York, 91-194. http://dx.doi.org/10.1142/9789812815989_0002
- [41] Smet, J.H. (1998) Ballistic Transport of Composite Fermions in Semiconductor Nanostructures. In: Heinonen, O., Ed., *Composite Fermions: A Unified View of the Quantum Hall Regime*, World Scientific, New York, 443-491. http://dx.doi.org/10.1142/9789812815989_0007
- [42] Jain, J.K. (2000) *Physics Today*, **53**, 39-45. <http://dx.doi.org/10.1063/1.883035>
- [43] Halperin, B.I. (2003) *Physica E: Low-Dimensional Systems and Nanostructures*, **20**, 71-78. <http://dx.doi.org/10.1016/j.physe.2003.09.022>
- [44] Murthy, G. and Shankar, R. (2003) *Reviews of Modern Physics*, **75**, 1101-1158. <http://dx.doi.org/10.1103/RevModPhys.75.1101>
- [45] Haldane, F.D.M. (1983) *Physical Review Letters*, **51**, 605-608. <http://dx.doi.org/10.1103/PhysRevLett.51.605>
- [46] Halperin, B.I. (1984) *Physical Review Letters*, **52**, 1583-1586. <http://dx.doi.org/10.1103/PhysRevLett.52.1583>
- [47] Peierls, R.E. (1955) *Quantum Theory of Solids*. Oxford University, London.
- [48] Sasaki, S. (2004) *Surface Science*, **566-568**, 1040-1046. <http://dx.doi.org/10.1016/j.susc.2004.06.101>
- [49] Sasaki, S. (2005) Binding Energies and Spin Polarizations of Fractional Quantum Hall States. In: Norris, C.P., Ed., *Surface Science: New Research*, Nova Science Publishers, Hauppauge, 103-161.
- [50] Sasaki, S. (1996) *Physical Review E*, **53**, 168-178. <http://dx.doi.org/10.1103/PhysRevE.53.168>